**33RD CONGRESS
OF THE INTERNATIONAL COUNCIL
OF THE AERONAUTICAL SCIENCES
STOCKHOLM, SWEDEN, 4–9 SEPTEMBER, 2022**

ICAS
2022
SWEDEN

A Rapid Design Method for Quiet Spike of Supersonic Transport Aircraft

Li-Wen Zhang [1,2], Zhong-Hua Han [1,2], Jian-Ling Qiao [1,2], Yu-Lin Ding [1,2], Qing Chen [1,2], Wen-Ping Song [1,2]

[1]National Key Laboratory of Science and Technology on Aerodynamic Design and Research, Northwestern Polytechnical University, Xi'an, 710072, China
[2]Research Center for Environment-friendly Supersonic Civil Transport, Northwestern Polytechnical University, Xi'an, 710072, China

Abstract

The severe sonic boom remains a great challenge for the return of supersonic transport aircraft to market. Among the sonic boom reduction methods, quiet spike technology is still one of the most effective ways during the last two decades. The quiet spike design studies were carried out by combining the near-field computational fluid dynamics (CFD) simulation with the far-field waveform parameter method. However, employing the expensive CFD method to obtain a near-field waveform is very time-consuming for a complex supersonic aircraft. Meanwhile, a low-fidelity waveform parameter method could not predict rise time. This paper proposes a rapid method for the design of a quiet spike, with the goal of reducing sonic boom intensity for a conceptual design stage. The design optimization method is used in the shape design of a spike-mounted configuration. For sonic boom prediction, the modified linear theory is utilized to partially replace the time-consuming CFD method to rapidly obtain near-field waveform, and then the augmented Burgers equation is solved for predicting the far-field signature. Validations of the modified linear theory for sonic boom prediction and CFD simulation are performed by using a NASA cone and a delta-wing-body configuration, respectively. The far-field sonic boom prediction method is validated by comparison with flight test data of an F-5E aircraft. The proposed method is then applied to design the quiet spike for a supersonic aircraft. Results show that the ground on-track sonic boom intensity can be reduced by 3.3 PLdB, compared with that of the baseline configuration.

Keywords: Sonic boom; Quiet spike; Sonic boom reduction; Modified linear theory; Design optimization

1. Introduction

A new generation of environment-friendly supersonic aircraft is one of the most promising directions for future civil transports, since it can significantly improve travel efficiency. However, the severe sonic boom remains a great challenge for the return of supersonic transport aircraft to market, after the last flight of Concorde in 2003. To reduce sonic boom intensity to an acceptable level, many efforts have been made since the last century. Among the sonic boom reduction methods, quiet spike technology [1], proposed by Gulfstream Aerospace, is still one of the most efficient ways to date.

The quiet spike technology consists of a set of telescoping spikes that extend forward from the nose of an aircraft during supersonic cruising. A series of weak shocks, which do not coalesce during propagation to the ground, are produced by spikes to prevent forming an intense nose shock, thereby reducing sonic boom intensity. Systematic studies of the quiet spike, such as aerodynamic and structural analysis [2], were conducted since the technology was proposed. For the influences on the sonic boom, several wind-tunnel tests [3][4] and F-5B flight tests [6][7] were carried out, confirming that near-field waveform could be shaped via quiet spike. Researchers [8]-[10] investigated the effect of spike parameters on sonic boom, finding that a quiet spike with a suitable length and fineness ratio could remarkably reduce sonic boom intensity. Design

optimization of an axisymmetric spike attaching to a delta wing was investigated by Ozcer [11]. Results reveal that the overpressure magnitudes of the leading and trailing shocks could be reduced. Subsequently, he mounted a multi-stage spike on a more realistic configuration, the shaped sonic boom demonstrator (SSBD). A multi-objective optimization [12] was performed to minimize the peak and impulse of pressure separately while considering the drag coefficient.

However, some issues exist in the above-mentioned design optimization studies. First, applying the expensive computational fluid dynamics (CFD) method to predict a near-field sonic boom is very time-consuming for a complex supersonic aircraft, such as SSBD configuration, although a grid adaptation technique is used. On the one hand, the generation of a grid capable of accurately capturing shock systems will cost some time once a new shape of aircraft is obtained. On the other hand, solving Euler equations or Navier-Stokes equations to obtain a high-fidelity near-field waveform also costs plenty of time. Second, the fidelity of the far-field prediction method is insufficient for the current sonic boom analysis. Although the waveform parameter method [13] incorporates aircraft motion and atmospheric effects, the underlying physics of propagation was based on linear theory and a weak shock assumption, leading to an inability to predict the shock rise time [14]. According to the modified linear theory for sonic boom prediction [15], which is an extension of Whitham theory [16], volume and lift effects are two main factors that produce an intense sonic boom. For a spike, the volume effect dominates the sonic boom, therefore, employing the modified linear theory for sonic boom prediction can rapidly obtain a near-field waveform. Meanwhile, the accuracy of the near-field waveform is sufficient at the stage of conceptual design. As a result, there is a strong need to develop a rapid design method for the quiet spike of supersonic transport aircraft based on the modified linear theory, which motivates the research of this paper.

The objective of this paper is to develop an efficient and rapid method for the shape design of a quiet spike at the stage of conceptual design. For sonic boom analysis, the modified linear theory for sonic boom prediction is utilized in rapid near-field waveform prediction for a quiet spike, whereas the CFD method is used only to simulate baseline configuration. The augmented Burgers equation is solved to predict the far-field signature. A design optimization method is used to determine the optimal quiet spike parameters, with the minimum ground perceived acoustic level in decibels (PLdB) [17] as an objective. An SBO-type optimizer named SurroOpt [18]-[20] is used to explore the global optimum design optimization problem.

This paper continues in section 2 to introduce the methodology. In section 3, Validations of the modified linear theory and CFD method are performed by using a NASA cone and a delta-wing-body (DWB) configuration, respectively. The far-field sonic boom prediction method is validated by comparison with flight test data of an F-5E aircraft. Section 4 employs the proposed method to design a quiet spike for a supersonic aircraft configuration. The intensity of the on-track sonic boom on the ground for the baseline and spike-mounted configuration is compared. Section 5 concludes this paper.

2. Methodology

2.1 Framework of A Rapid Design Method for Quiet Spike of Supersonic Transport

A rapid design method for a quiet spike of supersonic transport aircraft is proposed in this paper. Figure 1 depicts the framework of this method.

The near-field waveform for the supersonic aircraft configuration attached with a spike is reconstituted by combining spike shocks predicted by the modified linear theory with shock systems of baseline configuration simulated by the CFD method. The modified linear theory for sonic boom prediction is described in section 2.2. Notably, the CFD method is used only once in an entire framework for a baseline configuration simulation. The augmented Burgers equation is solved to predict the high-fidelity far-field signature, and it will be introduced in section 2.3. Meanwhile, a single-objective design optimization is carried out to determine a low-boom near-field waveform and spike shape parameters. Specifically, this approach can be divided into three steps.
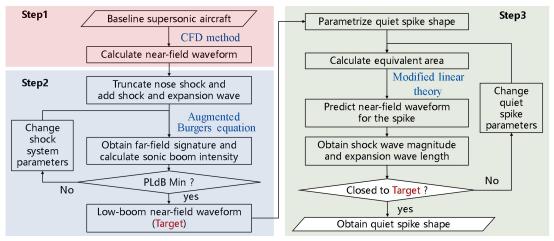
Figure 1 – Framework of a rapid method design for the quiet spike

1) The first step is to simulate a near-field waveform for the baseline supersonic aircraft using the CFD method. In this paper, Euler equations are solved to obtain the flow field. A Roe upwind scheme for space discretization with a Minmod limiter, and a lower-upper symmetric Gauss-Seidel (LU-SGS) implicit method in time marching are used.

2) The second step is to design a low-boom near-field waveform combining design optimization and high-fidelity far-field prediction methods. Comparing the near-field waveforms of the spike-mounted configuration with baseline, a main discrepancy is a series of weak shocks produced by the spike in the front of the waveform. In view of that the nose shock has little impact on the shock system downstream, the feature of the shock system produced by the leading-edge of the wing and aft-fuselage maintains to a great extent. Therefore, it is feasible and rapid to reconstitute a near-field waveform by combining spike shocks with the shock system of baseline configuration, replacing that simulated by the time-consuming CFD method. To obtain a reconstituted near-field waveform, the baseline configuration nose shock is truncated and shock and expansion waves are added ahead of the rest near-field waveform, corresponding to cutting the aircraft nose and adding a spike, respectively, as shown in Figure 2. The magnitude of shock waves and the length of expansion waves are used to parametrize the addition shock system. Subsequently, a low-boom near-field waveform is designed as a target for step three. The objective is PLdB, and the design variables are the parameters of the addition shock system. The SurroOpt is used for design optimization. The initial sample points are generated by a Latin hypercube sampling (LHS) method, and infill sampling criteria are the minimizing surrogate prediction (MSP), expected improvement (EI), probability of improvement (PI), mean squared error (MSE), and lower confidence bounding (LCB) methods. According to the optimal low-boom near-field waveform, the target magnitude of shock wave and length of expansion wave can be obtained.
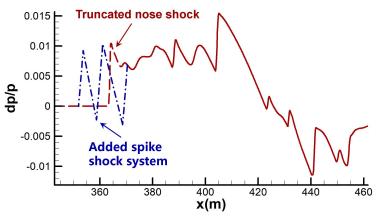

Figure 2 – Sketch of a reconstituted near-field waveform

3) The third step is to inverse design a spike shape to match the target low-boom near-field waveform using design optimization. The modified linear theory is employed to calculate near-

field waveform for a revolution spike, replacing the traditional time-consuming CFD method. For the modified linear theory, an assumption that the equivalent area distribution due to volume can be regarded as the total equivalent area distribution is made, since the volume effect is a dominant factor to produce sonic boom. The equivalent area distribution due to volume for a quiet spike of revolution shape, consisting of conic and cylindrical sections, is analytical. As a result, spike shock can be calculated directly according to spike parameters. Subsequently, a quiet spike shape design optimization is performed via SurroOpt optimizer, to match the target low-boom near-field waveform in terms of shock wave magnitude and expansion wave length. In the end, a quiet spike shape can be obtained.

2.2 The modified linear theory for sonic boom prediction

The modified linear theory for sonic boom prediction is built on the Whitham theory, which is widely used in supersonic aircraft conceptual design to date. According to this theory, sonic boom is caused by the volume and lift effects, thereby a function called F-function including these effects is constructed. F-function reflects the distribution of the source magnitude along the aircraft, which is significant for sonic boom prediction. Specifically, near-field waveform prediction based on the modified linear theory can be divided into three parts.

1) Obtain the total equivalent area distribution $S(x)$, which is a superposition of the equivalent area distribution due to volume $S_V(x)$ and lift $S_L(x)$. For the equivalent area distribution due to volume $S_V(x)$, it is obtained from the intersection area of the Mach plane and an aircraft, as shown in Figure 3. While the equivalent area distribution due to lift $S_L(x)$ is computed using lift distribution $L(x)$, which is given by equation (1). Notably, $L(x)$ is a superposition of the lift cut also by Mach plane along the axis.

$$S_L(x) = \frac{B}{\gamma p_\infty Ma^2} \int_0^x L(x)\mathrm{d}x \tag{1}$$

where p_∞ and Ma are the freestream pressure and Mach number, respectively. γ is the ratio of specific heats, and $B = \sqrt{Ma^2 - 1}$.

For a revolution spike consisting of conic and cylindrical sections, the volume effect is far more significant to produce an intense sonic boom compared with the lift effect. As a result, equivalent area distribution due to volume could be regarded as the total equivalent area distribution. Based on the length and diameter of the conic and cylindrical sections, the equivalent area distribution due to volume $S_V(x)$ can be calculated analytically. For a single-stage spike of the revolution shape as shown in Figure 4, the formula calculating $S_V(x)$ is given by equation (2).

$$S_V(x) = \begin{cases} \pi \cdot (\tan\beta)^2 \cdot (1 - (\tan\beta/\tan(\mu-\alpha))^2)^{-3/2} \cdot x^2 & (0 \le x < x_1) \\ (\tan\beta)^2 \cdot (1 - (\tan\beta/\tan(\mu-\alpha))^2)^{-3/2} \cdot (f_2(x) - \sin(f_2(x))) & \\ \quad \cdot x^2 + D^2 \cdot f_3(x) - |f_1(x)| \cdot \sqrt{0.25D^2 - f_1^2(x)} & (x_1 \le x < x_2) \\ 0.25\pi \cdot D^2 & (x_2 \le x < x_3) \end{cases} \tag{2}$$

where β, μ and α are the half top angle of the cone, Mach angle, and angle of attack, respectively. L_1 and L_2 are the length of conic and cylindrical section, and D is the diameter of cylindrical section. x_i $(i=1,2,3)$ are three locations which are depicted in Figure 4, and f_i $(i=1,2,3)$ are three factors given by equation (3).

$$x_1 = L_1 - D / 2 \tan(\mu - \alpha)$$
$$x_2 = L_1 + D / 2 \tan(\mu - \alpha)$$
$$x_3 = L_1 + L_2 - D / 2 \tan(\mu - \alpha)$$
$$f_1(x) = (x - L_1) \cdot \tan(\mu - \alpha)$$
$$f_2(x) = 2 \arccos(f_1(x))$$
$$f_3(x) = \pi - \arccos(f_1(x))$$

(3)

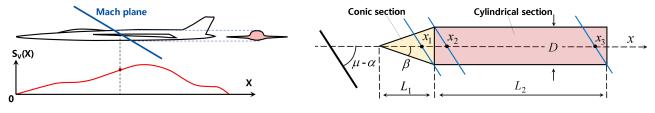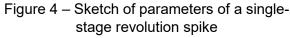To be noted, equation (2) can be extended to a multi-stage spike of revolution shape.

Figure 3 – Sketch of calculation for the equivalent area distribution due to volume

Figure 4 – Sketch of parameters of a single-stage revolution spike

2) Sonic boom F-function $F(y)$ is calculated utilizing the total equivalent area distribution $S(x)$, which is of the form

$$F(y) = \frac{1}{2\pi} \int_0^y \frac{S_V''(x)}{\sqrt{y-x}} dy$$

(4)

3) Once F-function is obtained, the near-field waveform can be calculated by Whitham theory, expressed by equation (5).

$$\frac{dp}{p_\infty}(y) = \frac{\gamma Ma^2}{\sqrt{2Br}} F(y)$$

(5)

where r is the distance away from the axis of the aircraft. Note that the nonlinear effect of shock system propagation should be considered before calculating near-field waveform. In general, a Burger-Hays method or an area-balanced method is normally employed.

2.3 Augmented Burgers Equation

To consider atmospheric effects on sonic boom propagation to the ground, the augmented Burgers equation, which is shown in equation (6), is widely solved in recent years. The terms in the right hand of the equation successively represent the effects of geometric acoustics spreading and atmospheric stratification, nonlinearity, thermoviscous absorption, and molecular relaxation processes. The augmented Burgers equation is solved by using an operator-splitting strategy, which allows us to solve each atmospheric effect separately with an appropriate numerical discretization method based on physical effects.

$$\frac{\partial P}{\partial \sigma} = -\frac{1}{2G} \frac{\partial G}{\partial \sigma} P + P \frac{\partial P}{\partial \tau} + \frac{1}{\Gamma} \frac{\partial^2 P}{\partial \tau^2} + \sum_j \frac{C_j}{1 + \theta_j \frac{\partial}{\partial \tau}} \frac{\partial^2 P}{\partial \tau^2}$$

(6)

In the above equation,
1) P is the dimensionless acoustic pressure with the reference pressure, and σ is the dimensionless coordinate in the main propagation direction.
2) τ is the dimensionless time of an acoustic signature to be propagated.
3) Γ is the thermo-viscous absorption parameter.

4) C_j is the dimensionless dispersion parameter of the *j-th* molecular relaxation process, and θ_j is the dimensionless relaxation time of the *j-th* molecular relaxation process.

The effects of geometric acoustics spreading and atmospheric stratification are handled by an analytic form. The term reflecting the nonlinear effect is solved using a Poisson analytic solution and a Burger-Hays method. Terms reflecting thermoviscous absorption and molecular relaxation processes are solved by a Crank-Nicolson difference scheme. An in-house code called bBoom [21]-[23] developed by the authors' research group is used in this paper.

3. Validation

For near-field waveform prediction, the modified linear theory and CFD simulation are validated by the NASA cone model #1 and a DWB configuration, respectively. While the F-5E aircraft flight test data is used to validate far-field sonic boom signature prediction.

3.1 Validation of the Modified Linear Theory for Sonic Boom Near-Field Prediction

A series of cones of different shapes were investigated in the NASA Langley 4×4 supersonic pressure tunnel [24], and these models are widely used to validate near-field waveform prediction methods [25]-[28].

NASA cone model #1 is a revolution shape consisting of a cone section and a cylindrical section. The length *L* of the cone section is 5.08 cm, and the diameter of the cylindrical section is 0.2866 cm. The modified linear theory is employed under conditions of the angle of attack $\alpha=0°$ and extraction location *H/L=10*. The equivalent area distribution due to volume is calculated using equation (2). A Burger-Hays method is utilized to determine the locations of shocks. The comparisons of the predicted near-field waveform using the modified linear theory with experiment data [24] are shown in Figure 5 and Figure 6 under the conditions of Mach number Ma=1.26 and 1.41, respectively. The predicted waveforms show an overall good match of the nose shocks, with little variations in the rear shocks.
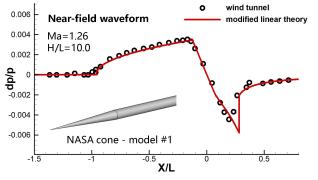
Figure 5 – Comparison of the predicted near-field waveform using modified linear theory with experiment data (*Ma=1.26, H/L=10.0*)
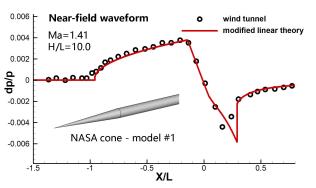
Figure 6 – Comparison of the predicted near-field waveform using modified linear theory with experiment data (*Ma=1.41, H/L=10.0*)

3.2 Validation of CFD Method for Sonic Boom Near-Field Prediction

A DWB configuration is proposed in the first AIAA Sonic Boom Prediction Workshop and it is widely used in sonic boom studies [29][30]. The model is longitudinally symmetric, consisting of a 69° leading-edge swept delta wing. The airfoil is diamond-shaped, with a 5% maximum thickness located at 50% chord. The total length of the wind tunnel test section is 0.1752 m, and Figure 7 shows a sketch of a half-model.

CFD simulation is carried out by solving the three-dimensional Euler equations with freestream Mach number *Ma*=1.70 and angle of attack $\alpha=0°$. A Roe upwind scheme for space discretization with a Minmod limiter, and a lower-upper symmetric Gauss-Seidel (LU-SGS) implicit method in time marching are used. Figure 8 compares the predicted on-track near-field sonic boom with data submitted by participants and experiment data [31]. Results show that it reveals an overall good match of shock systems compared with the submission of some participants, especially the shocks generated by the nose and wing. For the comparison with experiment data, some rounding of

shocks in the experiment is expected due to model vibration and fixed rail orifice spacing [29].
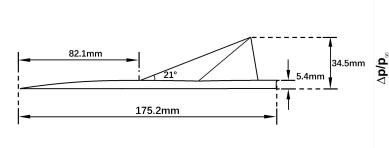
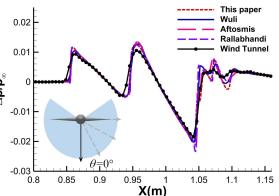Figure 7 – Sketch of DWB model test section

Figure 8 – Comparison of the predicted near-field waveform with data submitted by participants and experiment data [31]

3.3 Validation of Far-Field Sonic Boom Prediction

For the validation of far-field sonic boom prediction, flight test data #06 [7] measured 25.60m beneath the F-5E aircraft is used, which is shown in Figure 9. The ground signature is predicted under the conditions of Mach number Ma=1.40 and flight altitude H=9.75 km in a standard atmosphere. Figure 10 depicts the comparison of the predicted signature and the data observed on the ground [32]. It shows an overall good agreement with flight test data in terms of the amplitude and location of nose and tail shocks.
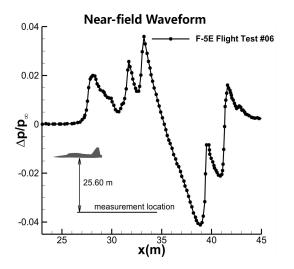
Figure 9 – F-5E military aircraft near-field waveform #06 [7] measured in the flight test
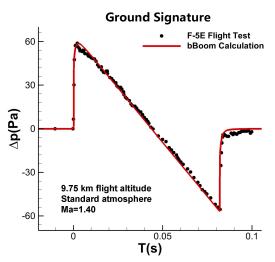
Figure 10 – Comparison of the ground signature predicted by bBoom code and the data observed on the ground [32]
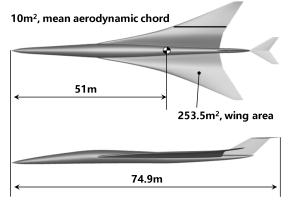
4. Application on a Supersonic Aircraft

4.1 Baseline Supersonic Aircraft Description

A supersonic aircraft configuration, which is designed by the authors' research group, serves as the baseline configuration, and the geometry is shown in Figure 11. The total length is 79.7m, with a fuselage length of L=71m. The wing area is 253.5 m^2, and the mean aerodynamic chord length is 10.0m. A T-wing is used in this configuration to increase the longitudinal length of lift distribution, which is beneficial to reduce sonic boom. Design conditions are Mach number Ma=1.6, and angle of attack $\alpha = 5.17°$.

For sonic boom evaluation, Figure 12 depicts the computational grid which consists of structured and unstructured regions. The aircraft has been rotated at an angle which is equal to the angle of

attack. The unstructured region is used for better capturing the highly nonlinear shock system near the aircraft, and the structured region is a conical shape of which the grid lines are aligned with Mach angle to reduce dissipation due to the computational grid in CFD simulation. The number of cells is approximately 12.7 million. Three-dimensional Euler equations are solved to obtain the flow field. The near-field waveform located at H/L=3.0 is extracted, as shown in Figure 13. Far-field propagation is carried out with the standard atmosphere, the flight altitude H=18.592 km, the interpolating frequency for the input signature of 1200 kHz, and the dimensionless marching step of 0.1 in the spatial direction. Based on the far-field signature shown in Figure 14, the on-track sonic boom intensity on the ground is 98.90 PLdB.
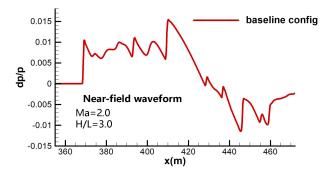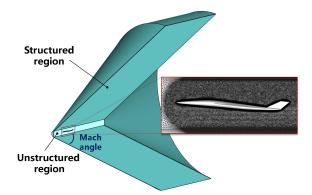

Figure 11 – Sketch of the baseline configuration

Figure 12 – Sketch of the computational grid for the baseline configuration

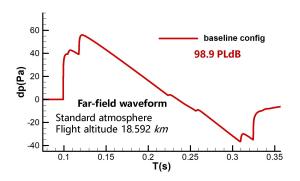Figure 13 – Near-field waveform for the baseline configuration

Figure 14 – Far-field signature for the baseline configuration

4.2 Target Low-Boom Near-field Waveform Determination

To obtain a target low-boom near-field waveform for a spike-mounted configuration, it needs to be reconstituted based on the baseline configuration. Figure 16 depicts the contour of the gradient of dimensionless overpressure dp/p_∞ along the direction $x - BH$, which could better reflect the propagation of the shock system. The propagation of nose shock and the subsequent shock is highlighted, and points A and B represent these two shocks. A near-field waveform is reconstituted by combining spike shocks with the shock system of baseline configuration, as shown in Figure 15. The specific reconstitution process is described as follows. The nose shock is first truncated corresponding to cutting section A-B in near-field waveform as a black dash line. For a single-stage spike, a spike shock system, consisting of a shock wave A_1-A_2 and an expansion wave A_2-A_3, is then added, and it is connected ahead of the rest near-field waveform. The addition of the spike shock system is marked as a blue dash-dot line. It is convenient to describe the addition shock system using two parameters P_S and L_E , which refers to the overpressure of spike shock and the length of spike expansion wave.

A design optimization method is utilized to determine a target low-boom near-field waveform with PLdB as an objective, in which the design variables are parameters P_S and L_E . The mathematical

model of the optimization problem is shown in equation (7). For far-field signature prediction, the setting parameters of bBoom code are the same as those in section 4.1. The SurroOpt is used for design optimization. The history of convergence is depicted in Figure 17. Based on the obtained low-boom near-field waveform, the values of the target magnitude of shock wave $P_{S,tar}$ and length of expansion $L_{E,tar}$ are 0.99 and 12.53, respectively, while the corresponding on-track sonic boom intensity is 95.41 PLdB.
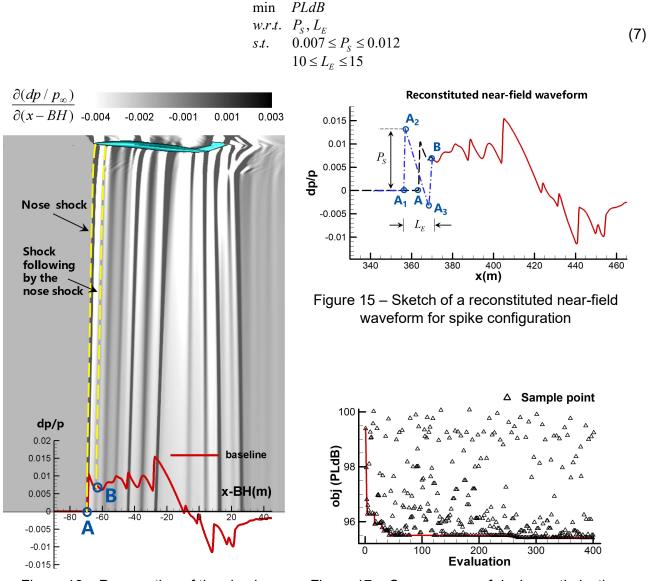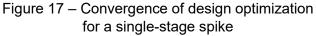
$$\begin{aligned}
&\min && PLdB \\
&w.r.t. && P_S, L_E \\
&s.t. && 0.007 \le P_S \le 0.012 \\
& && 10 \le L_E \le 15
\end{aligned} \tag{7}$$

Figure 15 – Sketch of a reconstituted near-field waveform for spike configuration

Figure 16 – Propagation of the shock system for baseline configuration

Figure 17 – Convergence of design optimization for a single-stage spike
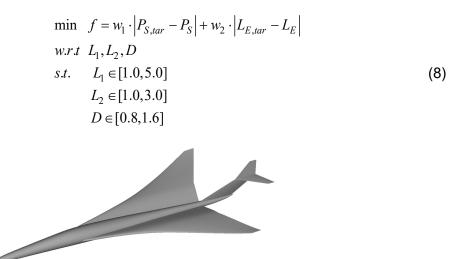
4.3 Shape Inverse Design of a Spike

A shape inverse design for a spike based on the modified linear theory is conducted using design optimization, to match the target low-boom near-field waveform provided from section 4.2. For a single-stage revolution spike which is made up of conic and cylindrical sections, the total equivalent area distribution in the modified linear theory is replaced by the equivalent area distribution due to volume, which could be calculated analytically as described in section 2.2. Near-field waveform thereby can be rapidly obtained by employing the modified linear theory, instead of the time-consuming CFD simulation. For CFD simulation, a grid of 12.7 million cells is computed using three nodes on TianHe-1A of the National Supercomputer Center in Tianjin. A single node comprises an Intel Xeon CPU E5-2690 14-core processor running at 2.60GHz, with 128GB of memory and 28 processes. Table 1 compares the near-field waveform calculation time of employing the modified linear theory with the CFD method. The result shows that employing the

modified linear theory can rapidly obtain a near-field waveform.

Table 1 – Sketch of the designed spike configuration

Methods	Calculation time of the near-field waveform
Modified linear theory	0.35s
CFD simulation	14h 45min

The mathematical model of the single-objective optimization problem is shown in equation (8), where w_1 and w_2 are the weight factors. In this paper, the weight factors w_1 and w_2 are given by 0.8 and 0.2, respectively. The design space of the diameter of the cylindrical section D is given based on the diameter of the truncated nose of the baseline configuration. The SurroOpt optimizer is used, and the number of evaluation steps is 200. Results show that it matches the target $P_{S,tar}$ and $L_{E,tar}$ when (L_1, L_2, D) is (3.5m, 4.8m, 1.4m). The location where the diameter is 1.4m along the baseline configuration is founded, and the single-stage revolution spike is added to obtain the spike-mounted configuration. The sketch of the inverse-designed spike-mounted configuration is depicted in Figure 18.

$$\min \quad f = w_1 \cdot \left| P_{S,tar} - P_S \right| + w_2 \cdot \left| L_{E,tar} - L_E \right|$$
$$w.r.t \quad L_1, L_2, D$$
$$s.t. \quad L_1 \in [1.0, 5.0] \tag{8}$$
$$L_2 \in [1.0, 3.0]$$
$$D \in [0.8, 1.6]$$

Quiet spike

Figure 18 – Sketch of the designed spike configuration

4.4 Sonic Boom Evaluation for the Designed Spike Configuration

In this section, a sonic boom analysis is performed using the high-fidelity methods to evaluate the spike-mounted configuration. The near-field waveform is simulated by the CFD method, and a comparison of the near-field waveforms of the baseline and spike-mounted configuration is shown in Figure 19. It is observed that there exists a significant discrepancy in the front of the waveform, compared with the rest of the shock system. The augmented Burgers equation is solved to obtain the on-track sonic boom far-field signature, as shown in Figure 20. For the baseline configuration, the nose shock merges with the following shocks according to the far-field signature. For the spike configuration, Figure 21 depicts the shock system coalescence during propagation to the ground. It can be seen that the spike shock does not coalesce with the following shocks, resulting in multi-stage shocks at the nose in the far-field. The sonic boom intensity for the spike-mounted configuration is reduced by 3.3PLdB compared with the baseline configuration. As a result, using such a principle, it is expected that a more significant sonic boom reduction can be achieved by attaching a multi-stage spike ahead of the baseline configuration.
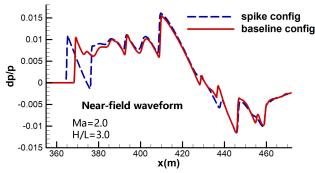
Figure 19 – Near-field waveform comparison for the baseline and spike configuration
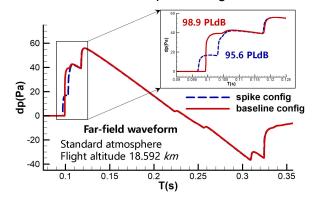

Figure 20 – Far-field waveform comparison for the baseline and spike configuration
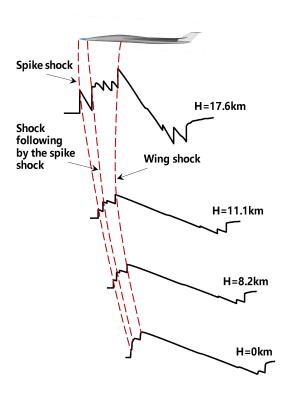

Figure 21 – Shock system coalescence during propagation to the ground for the spike configuration

5. Conclusion

A rapid method for the shape design of a quiet spike was proposed toward sonic-boom reduction in this paper. The modified linear theory was utilized to rapidly predict near-field waveform for a quiet spike, partially replacing the time-consuming CFD method. The CFD method was only employed for simulating the baseline supersonic aircraft flow field. A high-fidelity far-field signature was predicted by solving the augmented Burgers equation. Single-objective design optimization was first conducted to determine the target low-boom near-field waveform, with the minimum ground PLdB serving as an objective. The shape inverse design of a spike-mounted configuration was then carried out to match the target using a reconstituted near-field waveform, which combines the spike shocks with the shock system of the baseline configuration.

A single-stage revolution spike was designed on a supersonic aircraft configuration using the proposed method. The on-track sonic boom intensity on the ground for the spike-mounted configuration can be reduced by 3.3PLdB compared with that of the baseline configuration, which proves the effectiveness of the proposed method for reducing sonic boom intensity.

6. Acknowledgment

7. Contact Author Email Address

Zhong-Hua Han, Professor, hanzh@nwpu.edu.cn, Corresponding author.

8. Copyright Statement

References

[1] Henne PA, Howe DC, Wolz RR. Supersonic aircraft with spike for controlling and reducing sonic boom, US Patent US6698684, 2003.

[2] Freund D, Simmons F, Howe DC, et al. Lessons Learned-Quiet Spike^{TM} Flight Test Program. *46th AIAA Aerospace Sciences Meeting and Exhibit*, Reno, Nevada, Vol. 1, AIAA 2008-130, pp 1-11, 2008.

[3] Howe DC. Improved Sonic Boom Minimization with Extendable Nose Spike. *43rd AIAA Aerospace Sciences Meeting and Exhibit*, Reno, Nevada, Vol. 1, AIAA 2005-1014, pp 1-10, 2005.

[4] Wayman T, Waithe KA, Howe DC. Near Field Acoustic Test on a Low Boom Configuration in Langley's 4 x 4 Wind Tunnel. *29th AIAA Applied Aerodynamics Conference*, Honolulu, Hawaii, Vol. 1, AIAA 2011-3331, pp 1-18, 2011.

[5] Wayman T, Hicks G, Merret J. Force and Moment Test on a Low Boom Configuration in Glenn's 8 x 6 Wind Tunnel. *29th AIAA Applied Aerodynamics Conference*, Honolulu, Hawaii, Vol. 1, AIAA 2011-3332, pp 1-11, 2011.

[6] Haering EA Jr, Murray JE, Purifoy DD, et al. Airborne Shaped Sonic Boom Demonstration Pressure Measurements with Computational Fluid Dynamics Comparisons. *43rd AIAA Aerospace Sciences Meeting and Exhibit*, Reno, Nevada, Vol. 1, AIAA 2005-0009, pp 1-35, 2005.

[7] Meredith KB, Dahlin JA, Graham DH, et al. Computational Fluid Dynamics Comparison and Flight Test Measurement of F-5E Off-Body Pressures. *43rd AIAA Aerospace Sciences Meeting and Exhibit*, Reno, Nevada, Vol. 1, AIAA 2005-6, pp 1-31, 2005.

[8] Feng XQ. The Research of Low Sonic Boom Mechanism and Design Method of Supersonic Aircraft [dissertation]. Xi'an: Northwestern Polytechnical University; 2014 [Chinese].

[9] Leng Y, QIAN ZS. A CFD Based Sonic Boom Prediction Method and Investigation on the Parameters Affecting the Sonic Boom Signature[J]. *Procedia Engineering*, No. 99, pp 433-451, 2015.

[10] Zhai RH, Zhou H. Numerical analysis of slender-rod used for reducing supersonic aircraft noise. *Advances in Aeronautical Science and Engineering*, Vol. 8, No. 2, pp 171-181, 2017.

[11] Ozcer IA, Kandil OA, Yagiz B. Parametric Study and Effect of Nose-Piece Attachment on Sonic Boom Mitigation. *45th AIAA Aerospace Sciences Meeting and Exhibit*, Reno, Nevada, Vol. 1, AIAA 2007-1243, pp 1-11, 2007.

[12] Ozcer IA, Kandil OA, Design optimization of nose geometry of F-5E aircraft for sonic boom mitigation. *47th AIAA Aerospace Sciences Meeting including the New Horizons Forum and Aerospace Exposition*, Orlando, Florida, Vol. 1, AIAA 2009-1053, pp 1-14, 2009.

[13] Thomas LC. Extrapolation of sonic boom pressure signatures by waveform parameter method. Washington DC; NASA, Langley Research Center, NASA TND6832, 1972.

[14] Rallabhandi SK. Advanced sonic boom prediction using the augmented Burgers equation. *Journal of Aircraft*, Vol. 48, No. 4, pp 1245-1253, 2011.

[15] Walkden F. The shock pattern of a wing-body combination, far from the flight path. *The Aeronautical Quarterly*, Vol. 9, No. 2, pp 164-194, 1958.

[16] Whitham G. The Flow Pattern of a Supersonic Project. *Communications on Pure and Applied Mathematics*, Vol. 3, No. 5, pp 301-347, 1952.

[17] Stevens SS. Perceived level of noise by Mark VII and Decibels (E). *Acoustical Society of America*, Vol. 51, No. 2, pp B575-B601, 1972.

[18] Han ZH. SurroOpt: a generic surrogate-based optimization code for aerodynamic and multidisciplinary design. *Proceedings of ICAS 2016*, Daejeon, Korea, Vol. 1, ICAS 2016-0281, pp 1-10, 2016.

[19] Han ZH, Goertz S, Zimmermann R. Improving variable-fidelity surrogate modeling via gradient-enhanced kriging and a generalized hybrid bridge function. *Aerospace Science And Technology*, Vol. 25, No. 1, pp 177-189, 2013.

[20] Han ZH, Xu CZ, Zhang L, et al. Efficient aerodynamic shape optimization using variable-fidelity surrogate models and multilevel computational grids. *Chinese Journal of Aeronautics*, Vol. 33, No. 1, pp 31-47, 2019.

[21] Qiao JL, Han ZH, Ding YL, et al. Sonic boom prediction method for supersonic transports based on augmented burgers equation. *Acta Aerodynamica Sinica*, Vol. 37, No. 4, pp 663- 674, 2019 [Chinese].

[22] Qiao JL, Han ZH, Song WP, Song BF. Development of sonic boom prediction code for supersonic transports based on augmented Burgers equation. *AIAA Aviation 2019 Forum*, Dallas, Texas, Vol. 1, AIAA 2019-3571, pp 1-19, 2019.

[23] Qiao JL, Han ZH, Zhang LW, et al. Far-field sonic boom prediction considering atmospheric turbulence effects: An improved approach. *Chinese Journal of Aeronautics* [Internet]. 2022. Available from: https://doi.org/10.1016/j.cja.2022.01.013.

[24] Carlson HW, Mack RJ, Morris OA. A Wind tunnel Investigation of the Effect of Body Shape on Sonic Boom Pressure Distributions. NASA TND-3106, 1965.

[25]Wintzer M, Nemec M, Aftosmis MJ. Adjoint-Based Adaptive Mesh Refinement for Sonic Boom Prediction. *26th AIAA Applied Aerodynamics Conference*, Honolulu, Hawaii, Vol. 1, AIAA 2008-6593, pp 1-19, 2008.

[26]Casper JH, Cliff SE, Thomas SD, et al. Assessment of Near-Field Sonic Boom Simulation Tools. *26th AIAA Applied Aerodynamics Conference*, Honolulu, Hawaii, Vol. 1, AIAA 2008-6592, pp 1-14, 2008.

[27]Gan JY, Zha GC. Near field sonic boom calculation of benchmark cases. *53rd AIAA Aerospace Sciences Meeting*, Kissimmee, FL, Vol. 1, pp 1-19, 2015.

[28]Qiao JL. On sonic boom prediction and low-boom design optimization for supersonic transports [dissertation]. Xi'an: Northwestern Polytechnical University; 2019: 73-74 [Chinese].

[29]Cliff SE, Durston DA, Elmiligui AA, Jensen JC. Computational and experimental assessment of models for the first AIAA sonic boom prediction workshop. *52nd Aerospace Sciences Meeting*, National Harbor, MD, Vol. 1, AIAA 2014-0560, pp 1-37,2014.

[30]Qiao JL, Han ZH, Song WP. An efficient surrogate-based global optimization for low sonic boom design. *Chinese Journal of Aeronautics*, Vol. 39, No. 5, pp 121736, 2018 [Chinese].

[31]Park MA, Morgenstern JM. Summary and statistical analysis of the first AIAA sonic boom prediction workshop. *32nd AIAA Applied Aerodynamics Conference*, Atlanta, GA, Vol. 1, pp 1-43,2014.

[32]Pawlowski JW, Graham DH, Boccadoro CH, et al. Origins and overview of the shaped sonic boom demonstration program. *43rd AIAA Aerospace Sciences Meeting and Exhibit*, Reno, Nevada, Vol. 1, AIAA 2005-5, pp 1-14, 2005.